Programme	CIP – Competitiveness for innovation
Type of Action	Pilot B
Project Title	An optical neuro-monitor of cerebral oxygen metabolism and blood flow for neonatology
Acronym	BabyLux
Project n.	620996

D3.3 REPORT ON DEMONSTRATION OF INDIVIDUAL MODULES AND PROTOTYPES

Work Package	WP3
Lead Partner	1-POLIMI
Contributing Partner(s)	1 PoliMi, 3 ICFO, 4 IPT, 5 HP, 6 PQ, 7 Loop
Security Classification	PU (Public)
Date	30/06/2015
Version	0.4

Document history

Version	Date	Comments	Authors
0.1	09/06/2015	Table of contents	D. Contini (PoliMi)
0.2	15/06/2015	Testing of DCS module	M. Pagliazzi (ICFO)
0.3	28/06/2015	Testing of TRS module and revision of the entire document	D. Contini (PoliMi)
0.4	30/06/2015	Final revision	A.Torricelli (PoliMi)

The work leading to these results has received funding from the European Community's CIP competitiveness and innovation framework program under grant agreement nº. 620996.

Table of Contents

Table of Figures and Tables

1. Executive Summary

This deliverable describes the work performed in the Task 3.3 *Demonstration of Individual Modules and Prototypes*. Measurements were performed on the two separate modules, one for TRS and one for DCS, designed and built up in WP2 (see deliverable D2.2), in order to verify their characteristics and achievable performances. These tests were performed on TRS module at PoliMi facilities and on DCS module at ICFO facilities, respectively. All the measurement were done employing the probe specifically designed for the BabyLux demonstrator and built by IPT. The results presented in this deliverable are also the basis of the following deliverable D3.4 concerning the characterization of the integrated systems.

2. Introduction

The aim of the Task 3.3 *Demonstration of Individual Modules and Prototypes* is verifying the consistency between the characteristics of the families of components chosen for the final demonstrator for both TRS and DCS modules and the overall performances of the two independent modules.

This document is divided into two parts: the first one for results related to TRS module based on 5 paragraphs one for each studied parameters (Linearity, Accuracy, Reproducibility, Depth selectivity and Noise level), and the second one for results related to DCS module based on 3 paragraphs one for each studied parameters (Linearity and Accuracy, Reproducibility, Depth selectivity).

A general conclusion on both TRS and DCS components is provided at the end of this document.

3. Demonstration of TRS Module

In the last ten years, different protocols were defined in order to characterize optical instrument in diffuse optics applications[1]. In the last years a particular attention was dedicated to time domain diffuse optics instruments[2]. We exploit these protocols in order to establish the performances of the TRS module of the BabyLux prototype.

3.1 Linearity

A set of 32 solid phantoms mimicking optical properties of tissues were measured. Phantoms are made by epoxy resin as solid matrix, TiO_2 particles as scatterers and ink powder as absorber.
This set of phantoms covers a range of optical properties very large: 0-0.49 cm^{-1} by steps of 0.07 cm^{-1} for the absorption coefficient (labelled from 1 to 8 respectively) and 0-20 cm^{-1} by steps of 5 cm^{-1} (labelled from A to D respectively) for the scattering coefficient. Nominal values for the optical parameters are defined at 660 nm. The covered range of optical properties is much larger than the *in vivo* variability for average optical properties of the head in new-borns.
Measurements are performed putting the BabyLux probe on the surface of each phantom and acquiring 5 TRS curves with an acquisition time of 1 s each at the three wavelengths at the same time.
The measurements were analysed by fitting the experimental data with an analytical theoretical model for homogeneous media and averaging the results for the five repetitions.
As example the results obtained for 690 nm are showed in the following Figures 1 and 2.

The system shows good linearity for both reduced scattering and absorption coefficient at 690 nm. At 830 nm the results are similar, while at 780 nm we observe a saturation of the retrieved results for absorption values higher than 0.2 cm^{-1}. This behaviour is related to the shape of the IRF at 780 nm. In consideration of the results obtained at 780 nm and in order to avoid crosstalk between TRS and DCS measurements (in the last design of the integrated instrument will be operate simultaneously) the 780 nm laser head will be substituted in the integrated system by a laser head operating at 760 nm. The new wavelength is sufficiently close to the old one to ensure that this characterisation can be representative also of the new one. A proper test of the new laser head will be carried out in the integrated system.

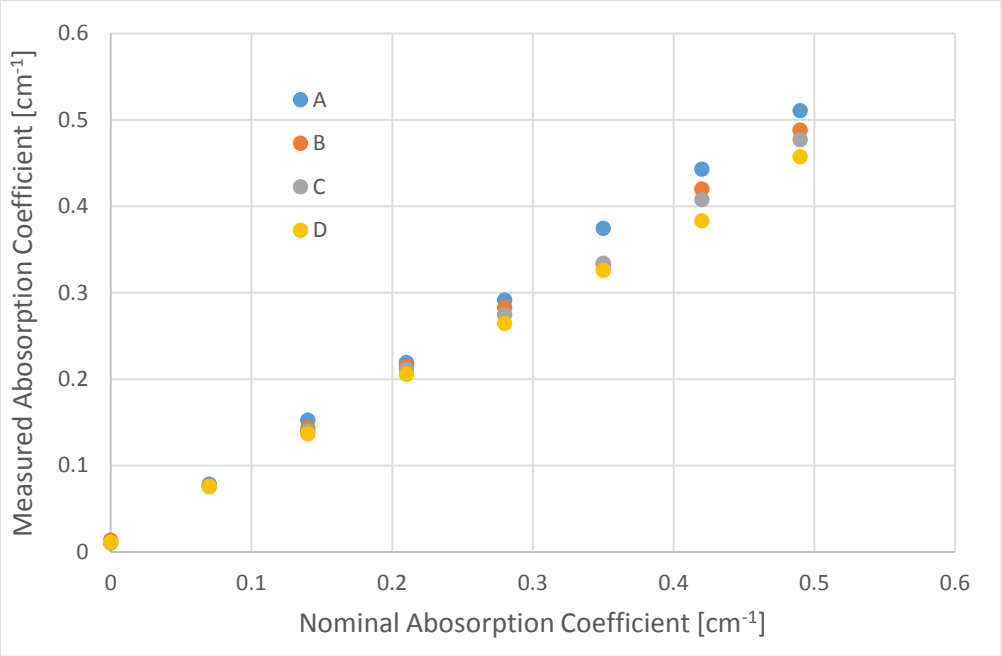

Figure 1: Linearity in absorption @ 690nm

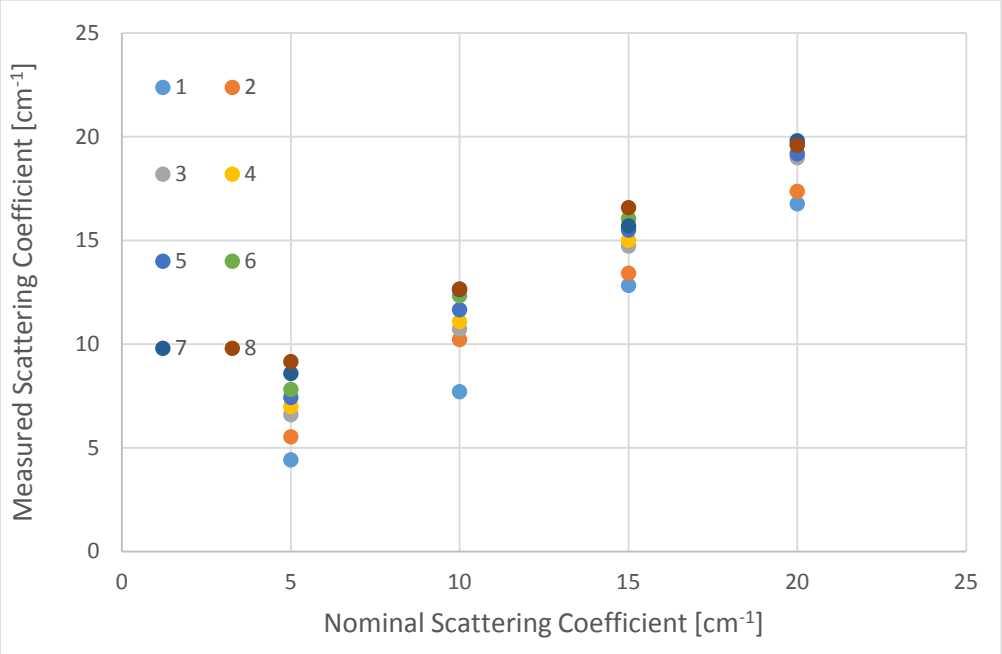

Figure 2: Linearity in scattering @ 690nm

3.2 Accuracy

The accuracy of the TRS module was evaluated by means of the same data set of the previous paragraph. Comparing the results obtained with the established true optical properties of the phantoms (measured by means of repetitive measurement with a state of the art TRS system) we obtained the following average errors (see Table 1):

Table 2: Average accuracy

	Absorption	**Scattering**
690 nm	5%	13%
780 nm	20%	15%
830 nm	10%	32%

In the averaged results were discarded the values of phantoms labelled 1 where the nominal absorption should be near zero.

Absorption is estimated more accurately than scattering apart at 780 nm, which shows some problems as highlighted in the previous paragraph.

The large average error for 830 nm in the estimation of scattering coefficient is probably due to the presence of some optical reflection, negligible to be highlighted by the IRF shape measurement but sufficient to degrade optical properties estimation. In the integrated system fibers length will be adjusted accordingly.

3.3 Test-to-test Reproducibility

We evaluated the test-to-test reproducibility of results of the TRS module during repetitive measurements taking into account also the variability due to the repositioning of the probe on the sample. In order to simulate a more realistic scenario all the measurements were done both on phantom and *in vivo* (on the head of an adult volunteer).

All the experiments were based on 10 measurement sessions during which 10 TRS curves were acquired with an integration time of 1 s each.

Four different experiments were conducted:

1) Placing the probe on a solid phantom (μ_a = 0.1 cm^{-1} and μ_s' = 10 cm^{-1}) repetetively (10 sessions).
2) Placing the probe on the head of an adult volunteer repetetively (10 sessions).
3) Fixing the probe on the same solid phantom of the first experiment acquiring the same total number of curves as in experiment 1.
4) Fixing the probe in the same positions of the head as in the second experiment acquiring the same total number of curves as in experiment 2.

The measurements were analysed by fitting the experimental data with an analytical theoretical model for homogeneous media and evaluating absorption and scattering coefficients.

The coefficient of variability intra-session (rows in Table 2) and inter-session (last row labelled Repeatability in Table 2) were computed for all the four experiments for three different parameters: absorption coefficient, reduced scattering coefficient and photon counts (see Table 2).

Table 2: CV of the measured parameters (μ_a, μ_s' and photon counts) during the four experiments for test-to-test reproducibility assessment. Values larger than 4% are in red.

	CV Absorption Coefficient			
	Repeated		Fixed	
Session	Head	Phantom	Head	Phantom
1	3%	1%	1%	1%
2	2%	1%	2%	2%
3	2%	2%	2%	2%
4	2%	2%	1%	2%
5	3%	2%	1%	1%
6	3%	3%	2%	2%
7	4%	6%	1%	2%
8	3%	4%	1%	2%
9	3%	1%	2%	2%
10	1%	3%	1%	2%
	Repeatability			
	3%	2%	1%	1%

	CV Scattering Coefficient			
	Repeated		Fixed	
Session	Head	Phantom	Head	Phantom
1	3%	1%	2%	1%
2	2%	1%	2%	1%
3	1%	2%	1%	2%
4	2%	1%	1%	2%
5	2%	2%	2%	1%
6	2%	3%	2%	3%
7	4%	5%	1%	2%
8	3%	4%	1%	2%
9	4%	2%	2%	2%
10	1%	2%	2%	2%
	Repeatability			
	2%	2%	1%	0%

	CV Photon Counts			
	Repeated		Fixed	
Session	Head	Phantom	Head	Phantom
1	1%	2%	3%	2%
2	1%	4%	4%	2%
3	2%	5%	3%	2%
4	8%	4%	1%	1%
5	2%	3%	2%	2%
6	1%	6%	2%	1%
7	2%	5%	3%	2%
8	8%	4%	2%	2%
9	5%	2%	3%	3%
10	6%	2%	3%	2%
	Repeatability			
	34%	52%	5%	3%

We can see that the repeatability between different measurements is very high, in fact CV is lower than 4% for both absorption and reduced scattering coefficients estimation. The intra measurement variability is more or less the same (few sessions show CV larger than 4%). The differences between repetitive experiments and the control ones, where the probe is fixed on the surface of the sample, are very low and thus ascribable to the repositioning of the probe. Looking at the third parameter (total counts) we can observe a larger intra- and inter-measurement variability. This can be explained because the optical contact between probe and sample is highly affected by the repositioning of the probe itself and on the fluctuations and mechanical instability of the contact, while the estimation of the optical properties is independent of the number of photons acquired (if the contrast to noise ratio is sufficient) but depends only on the shape of the time-resolved reflectance curve.

3.4 Depth specificity

A set of bi-layer solid phantoms mimicking optical properties of tissues were measured. Phantoms are made by silicon as solid matrix, TiO_2 particles as scatterers and ink powder as absorber.

A single geometry was considered: top layer 5 mm thick (mimicking extra-cerebral tissues) over a bulk layer of few centimetres of thickness (mimicking cerebral tissues). The optical properties of the two compartments were varied independently: for the top layer μ_a was 0.1 or 0.2 cm^{-1} and μ_s' was 5,10 or 15 cm^{-1}, while for the bulk layer μ_a was 0.05, 0.1 or 0.2 cm^{-1} and μ_s' was 5, 10 and 15 cm^{-1}. Different combinations of optical properties for top and bulk layers were tested. Measurements were performed placing the probe on the top layer of the sample and acquiring 5 TRS curves with an integration time of 1 s each at the three wavelengths at the same time.

The measurements were analysed by fitting the experimental data with an analytical theoretical model for homogeneous medium (two unknown μ_a and μ_s') and with an analytical model for bilayer medium (four unknown μ_a and μ_s' for both layers). The results were averaged over the five repetitions.

As example the results obtained at 690 nm with the homogeneous medium model are showed in Figures 3 and 4. In Figures 5 and 6 the results obtained with the bilayer model are shown.

Observing figures 3-6 it is possible to clearly verify that, in a bilayer structure, the system is able to retrieve and follow with a sufficient accuracy the absorption coefficient of the bottom layer and the scattering coefficient of the top layer, independently of the analysis method employed.

In the BabyLux instrument the TRS goal is duplex: quantifying brain tissue oxygenation related to brain optical properties (bottom layer optical properties) and providing optical properties of the investigated tissues in order to improve DCS accuracy. Looking at the results we can confirm the capability of the system to succeed in the first goal, but regarding the second goal we need to further investigate this issue in order to understand the impact to DCS accuracy and possible solution to the problem.

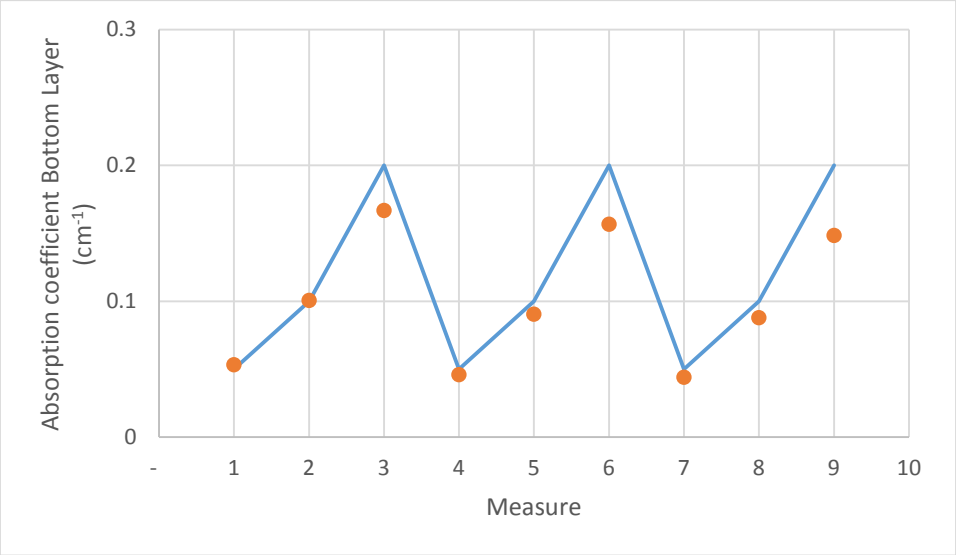

Figure 3: Estimated absorption coefficients (symbols) and nominal values (blue line) of the bottom layer: homogeneous model.

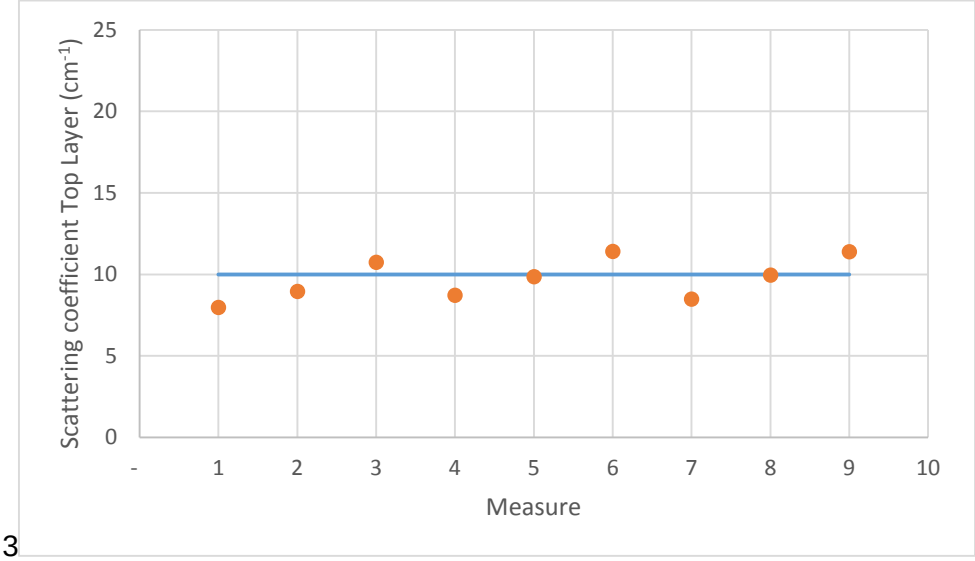

3

Figure 4: Estimated scattering coefficients (symbols) and nominal values (blue line) of the top layer; homogeneous model.

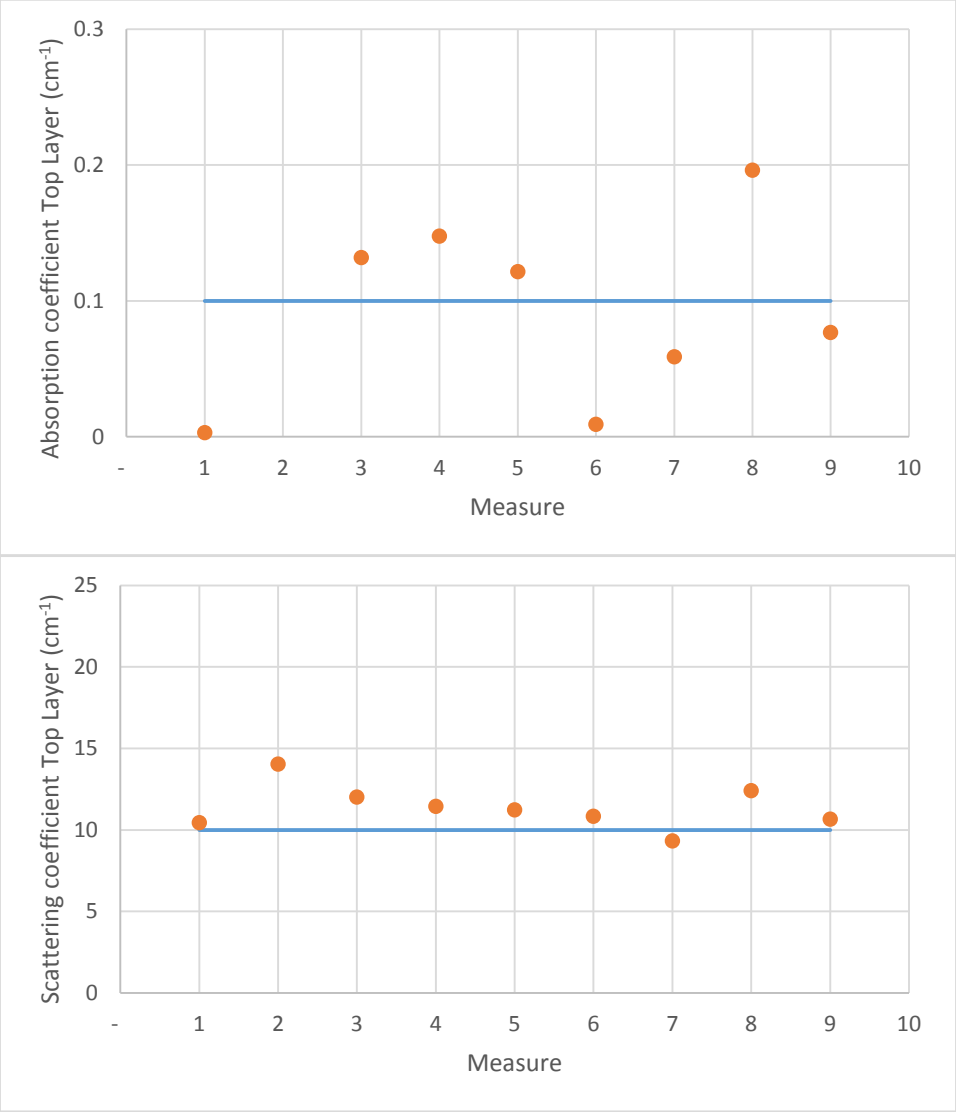

Figure 5: Estimated absorption and scattering coefficients (symbols) and nominal values (blue line) of the top layer

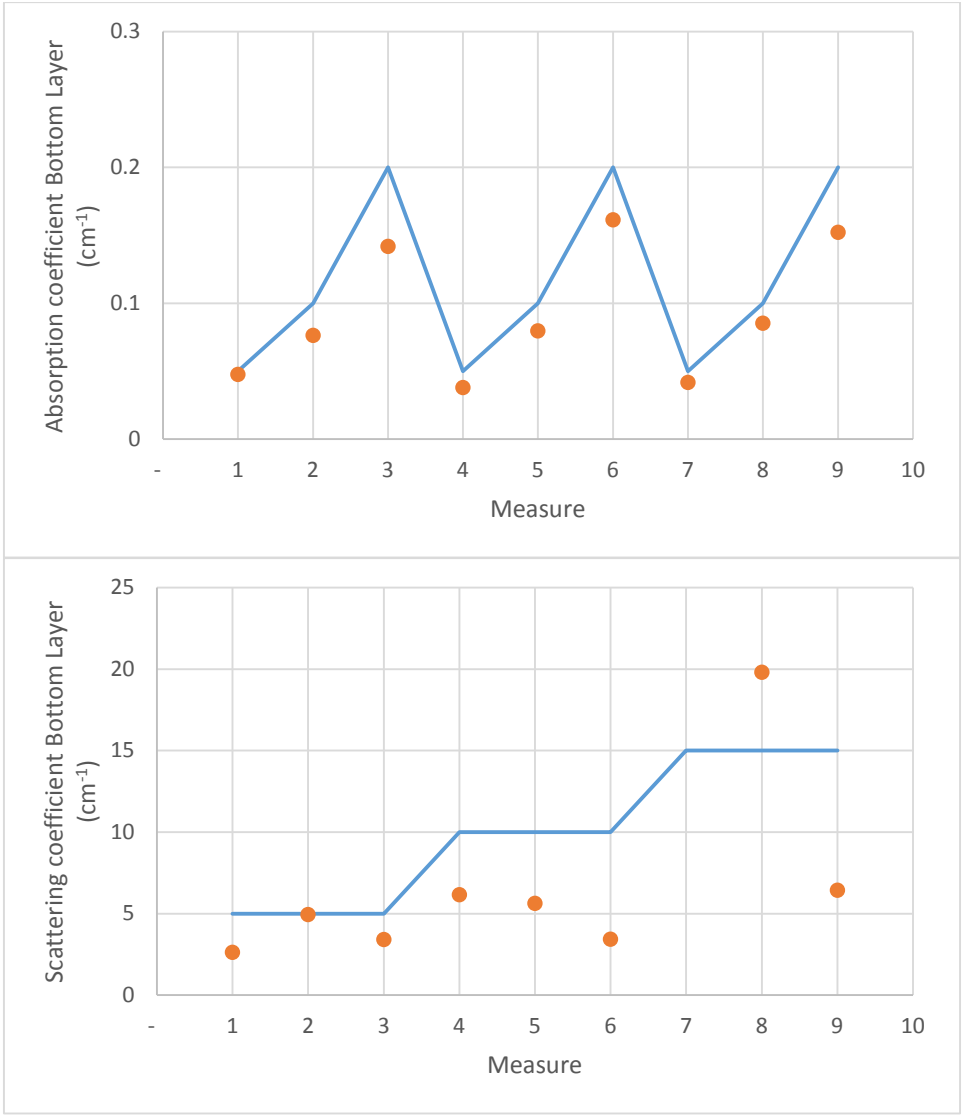

Figure 6: Estimated absorption and scattering coefficients (symbols) and nominal values (blue line) of the bottom layer

3.5 Noise level

A series of measurements was performed on a solid phantoms in order to identify the level of contrast to noise ratio achievable in the determination of the optical properties of a medium. The measurements were performed on an epoxy resin phantom (see paragraph 3.1) with μ_a = 0.1 cm^{-1} and μ_s' = 10 cm^{-1}. One hundreds time-resolved reflectance curves were acquired at different levels of photon counts. For each signal level the coefficient of variation was estimated. The intrinsic variability of the measurement represent the maximum achievable contrast at that specific level of signal and thus the sensitivity of the instrument. Results are shown in Figure 7.

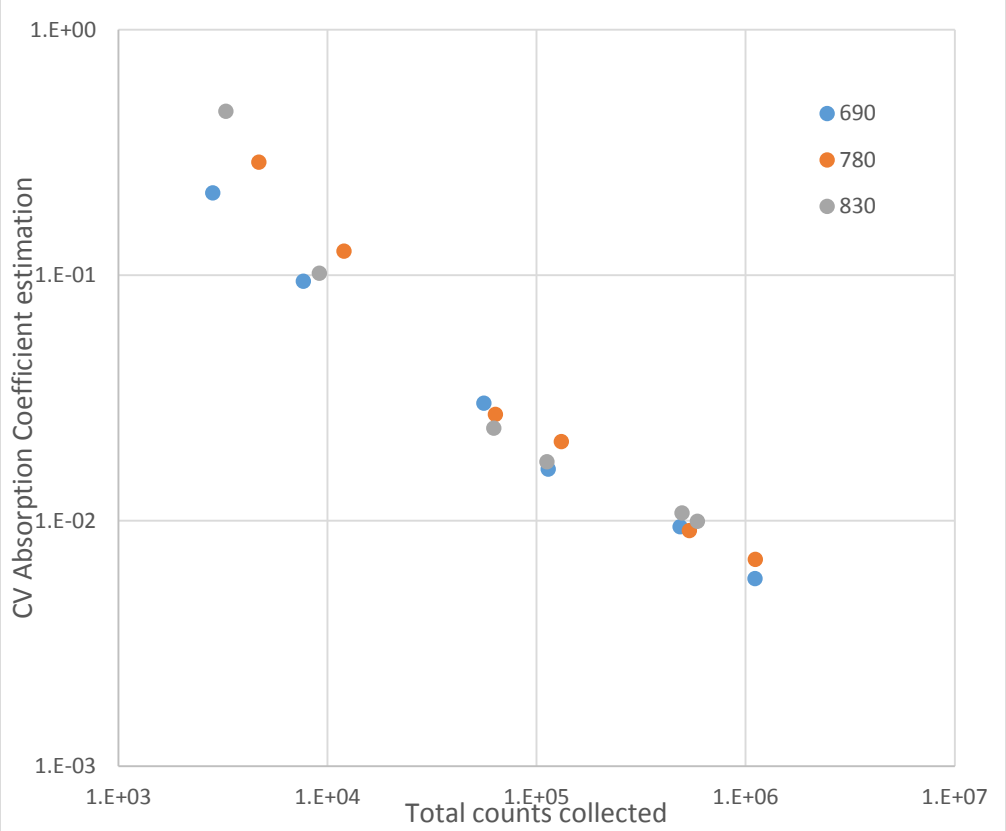

Figure 7: Variability of the estimation of the optical properties at various signal levels

Looking at Figure 7 we can estimate a sensitivity of 1% for the estimation of the absorption coefficient at the signal level larger than 500 kcounts. This level of signal is compatible with a typical *in vivo* measurement of BabyLux which is hypothesized to be last for a few seconds.

4. Demonstration of DCS Module

The first challenge in testing the day-to-day reproducibility of the DCS measurement is to obtain a dynamic phantom which is able to simulate the response of a biological tissue. To date, there is no proposed solution to this. An enclosure filled with a liquid, water based synthetic optical phantom was designed for the purpose (Fig 8). The liquid used here was a suspension of synthetic polymer and ink in water. The optical properties were adjusted to match the mean properties of premature baby head between 30 and 36 weeks of gestational age[3] (see Table 3).

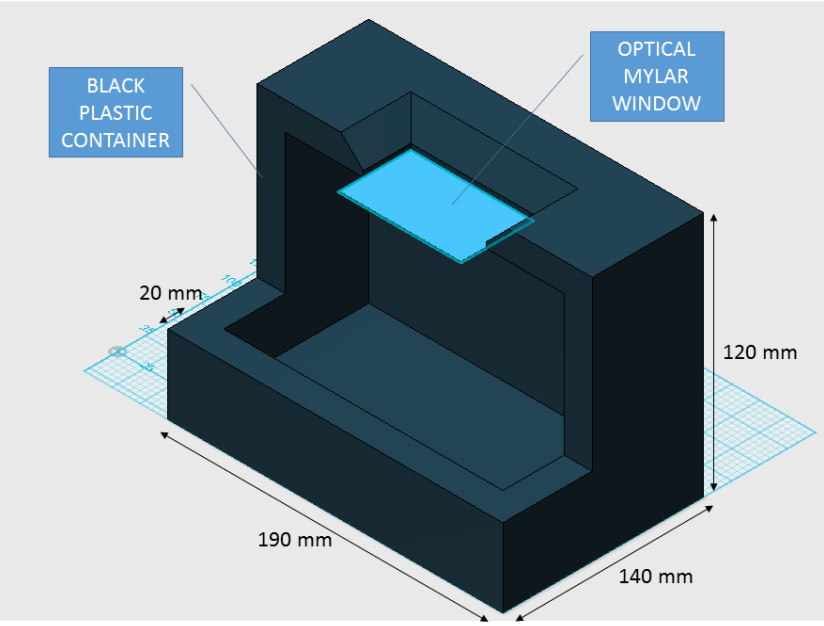

Figure 8: The container of the liquid phantom used for reproducibility assessment of the DCS module

Table 3: Optical properties of the phantom as measured by TRS-20 (Hamamatsu Photonics, Japan)

	μ_a, cm^{-1}	μ_s', cm^{-1}
Day 0	0.118	5.79
Day 20	0.101	5.12

The dimension of the container were carefully chosen to approximate a semi-infinite boundary condition for the propagation of TRS and DCS light. A transparent window was made with two thin Mylar sheets (0.25 mm, Dupont, USA) joint together by using a black tape spacer of 5 mm width. It has been glued on the upper side of it to ensure an optical aperture. The enclosure ultimately impeded the evaporation of the liquid and contaminations from the outside.
Brownian diffusion was probed almost daily for a month after shaking the box and letting it rest for 120 s, to counter balance possible but not certain irreversible sedimentation of the polymer that can happen on the long run (i.e. months). Despite the very same material used for the phantom was shown to give stable correlation curves over many hours (1.16% variation over 10 h), as showed in Deliverable 3.2, the phantom has a tendency to separate the polymer (solid) phase from water over days. That's reversible with a mild (40") shaking. Measurements were carried out with 1.5 s integration time for a variable number (2 to 10) of source replacements. A 3D printed probe hosting a fibre optic detector and source for a single DCS

channel at a distance of 1.5 cm was put in contact with the window, with the source and detector separated by the black tape spacer. This way, light could not channel directly through the window itself. Temperature was measured prior to DCS through the Mylar window with an infrared thermometer (Thermoworks, UK). DCS curves were excluded if the beta parameter was greater than 0.5 or smaller than 0.4, if the tail (τ > 6 msec) had values greater than 0.99 or smaller than 1.05 and if the count rate was lower than 100 kHz. One day (day 29) was excluded because the temperature was considerably higher at the moment of the measurement (25 °C) for sitting in a not air conditioned controlled room.
The optical properties (attenuation and reduced scattering coefficients, μ_a and μ_s' respectively) were determined from TRS measurements carried out in two occasions: when the phantom was built (day 0) and after 20 days, by using a TRS-20 device (Hamamatsu, Japan). The probe used had a source detector separation of 1.5 cm, and it was also placed straddling over the black spacer. Measurements showed limited variation of the properties in about a month of measurement, quantified in a mild decrease of μ_s' and μ_a of 12% and 15%, respectively.

4.1 Day-to-day reproducibility

By considering the first 30 s of acquisition (20 points) for each day, the daily mean variability is 4% (2%-7% range), which is considerably larger than the previous results from deliverable 3.2 (1% variation over 30 min). The test-retest variability, estimated by replacing the probe on the phantom, was evaluated, for each of the first 10 days by comparing the mean value of each repetition. Surprisingly, this resulted in a smaller mean variability of 2.7% (0.8%-4.8% range, see Table 4). These two findings seems to suggest that the probe attachment or the overall mechanical build of the phantom were not stable. With respect to the previous deliverable, also the optical properties of the phantom are changed and this can contribute. Further work is requested for reducing these two variabilities, which have to be attributed to a failure of the phantom. Nevertheless, the variability of each day mean over the whole epoch showed a coefficient of variation (standard deviation of daily means of the first 30 s over the overall mean value) of 7%. When considering the range of the daily means, this value reached 22%. The mean value of the estimated Brownian diffusion coefficient was $1.30 \cdot 10^{-8}$ cm2 s-1, corresponding to a typical decay time of the DCS curve (Γ) of $9 \cdot 10^{-5}$ s.

Table 4: Coefficient of variation of the estimated DB for probe replacement

Day 1	Day 2	Day 3	Day 4	Day 5	Day 6	Day 7	Day 8	Day 9	Day 10
2%	4.6%	4.8%	1.6%	3.3%	3.5%	1.1%	0.8%	3.4%	1.6%

The residual variability of the DCS signal recorded daily can be due either to the instability of the DCS module or to the phantom itself. Brownian diffusion in the phantom is known to be influenced by the temperature, which was found to be fairly constant during each measurement (23.1 ± 1 C), except for one rejected point (day 29). In any case the results show that the error is within the target tolerance (see Figure 9).

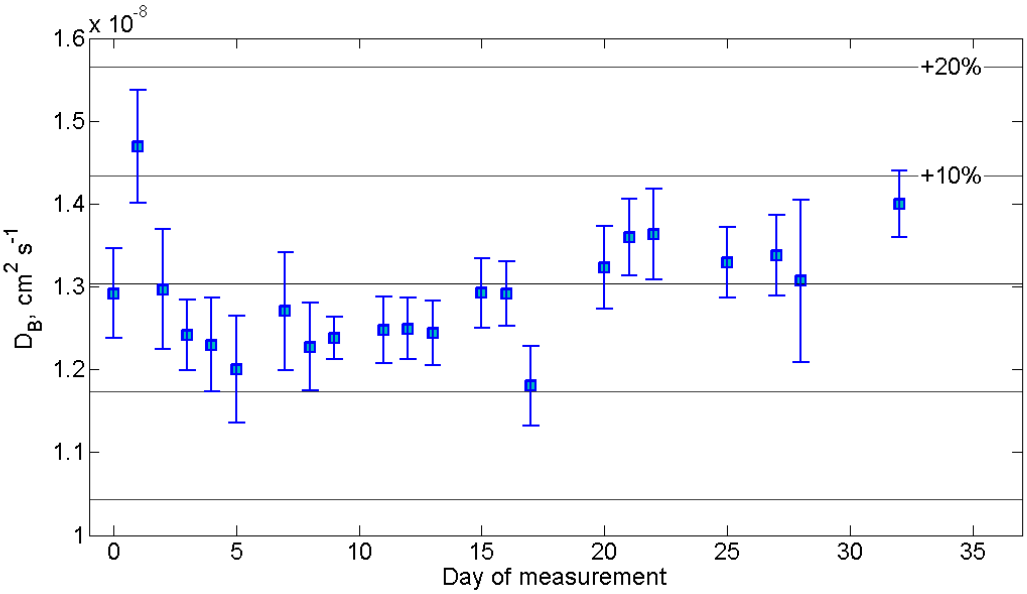

Figure 9: Results of the repeated measurements on the liquid phantom over a 32 day epoch. Values and errorbars represent the mean values and variability of the DCS signal in the first 30 s of measurement for each day

4.2 Linearity and Accuracy

Linearity was tested by moving a solid phantom (INO, Canada) with a translating stage (Thorlabs, DE) while measuring DCS with a probe ensuring a fibre positioning at 1.5 cm distance for an integration time of 1.5 s (see Figure 10).

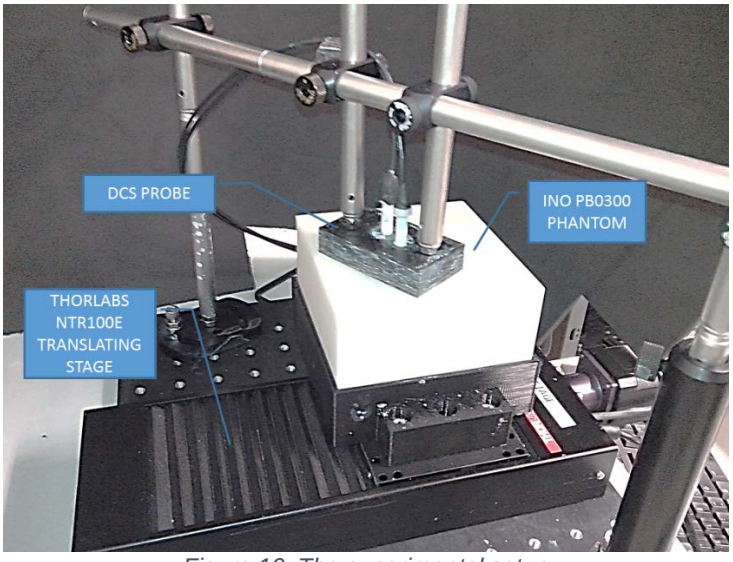

Figure 10: The experimental setup

The stage was moved the same day either in the positive (GO) or in the negative (abbreviated RETURN or RE) direction while measuring it with DCS. The phantom used had the optical properties reported in Table 5.

Table 5: Optical properties of the solid phantom used, measured by the manufacturer at 785 nm wavelength

μ_a (cm^{-1})	μ_s' (cm^{-1})
0.0999	9.97

Figure 11 shows the DCS estimated velocity versus translating stage velocity.

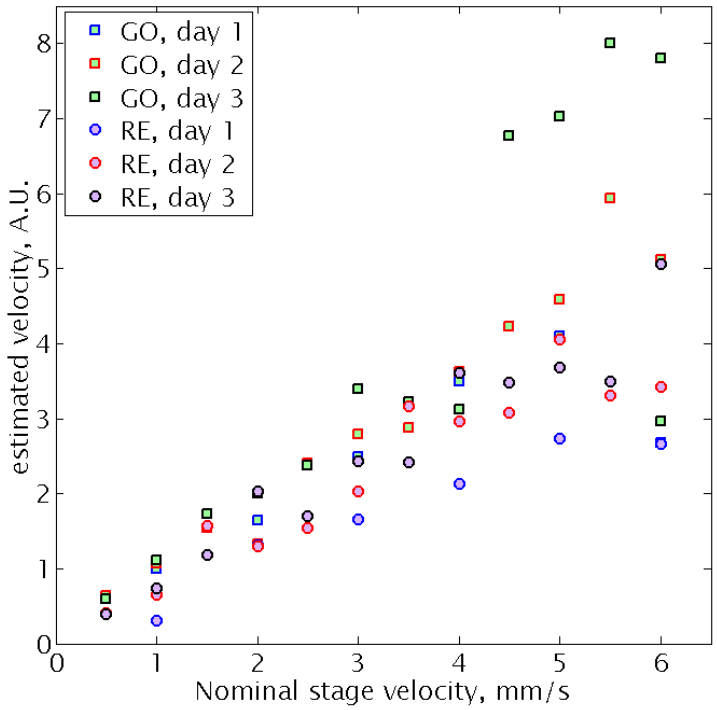

Figure 11: DCS estimated velocity versus translating stage velocity. (GO: translating stage moving towards positive direction; RE: moving towards negative direction)

By reporting nominal translating stage velocity and DCS-estimated velocity we could verify a high and significant degree of linearity. The test was repeated three times in three different days. DCS module was turned on and off between two subsequent measurement and the probe replaced, thus simulating ideal conditions of test-retest reproducibility.
Accuracy was tested by comparing the values obtained each day (Table 6). A coefficient of variation of 44.5% (maximum) with an average of 28.2% was obtained. When the stage is moving towards negative direction (RETURN), Table 7 reports R2 values > 0.88 when considering all the experimental points for each day. Day-to-day coefficients of variation for each nominal velocity are on the average within the target accuracy, as shown in Table 7, for most velocities. There are some points that anyway give worse results (coefficient of variation > 30%), especially at high velocities. We believe this is the effect of the lower time available for acquiring data when the stage is moving faster.

By looking at the typical decay time (Γ), defined at the correlation time at which the normalized electric field correlation reaches the 1/e value, at each stage velocity the curve shape can be compared with the shape of DCS curves that are typical on human subjects. On the overall,

this parameter varied between $2.69 \cdot 10^{-2}$ s and $2.63 \cdot 10^{-5}$ s, that for our target optical properties (see Table 3, first row) correspond to 10^{-10} to 10^{-7} cm^2 s^{-1} range in the estimated αDB.
The proposed solution looks promising, as it is fully mechanical and it allows to test linearity and accuracy over a broad range of curves shape that reproduce the decay times measured in physiological conditions. Failures in the accuracy at some points can be improved by improving the precision of the phantom build (i.e. testing other stage models) as well as increasing the acquisition time or by simply using phantoms of greater length, which now limits the points that can be acquired especially at high velocities of the stage.

Table 6: Coefficients of variation between three repetitions of the same experiment

Coefficient of Variation, %	**GO**	**RETURN**	**GO+RETURN**
Mean	18.3%	20.1%	28.2%
Range	51.2% - 0.7%	39.4% - 3.7%	44.5% - 12.5%

Table 7: Results of the linear fitting of the estimated velocity with respect to the nominal stage velocity

	Trans stage GO	**Trans stage RETURN**	**Trans stage GO**	**Trans stage RETURN**	**Trans stage GO**	**Trans stage RETURN**
R^2	0.61	0.93	0.96	0.88	0.68	0.93

4.3 Depth selectivity

A depth selective tissue phantom was judged unfeasible to make. Anyway, anatomical MRI data[5] showed that full term age (40 ± 4 weeks) children have a combined extra-cerebral layer thickness (scalp, skull and cerebrospinal fluid) of 0.74±0.1 cm. At a median age of 2.8 (interquartile range 3.0) years children with congenital heart defects showed a combined skull, scalp and cerebrospinal fluid thickness of 0.81 cm (interquartile range 0.28 cm) [6]. This is believed to further decrease in premature children, thus facilitating the light propagation through tissue and the ability to detect changes in deeper layers. DCS is intrinsically more sensitive to deeper layers than continuous wave near infrared spectroscopy of about a factor 6, as shown by simulation in the paper of Selb et al[4] for adults. This holds true for the adult head, and it is reasonably valid for the thinner newborn's scalp and skull. Intuitively, the reason for the increased contrast is that photons undergoing longer paths in tissue will be transferring more momentum to the scattering centres, thus contributing greatly to the loss of correlation, conversely with respect to NIRS where the same photons will be reaching the detector in lower numbers. In adults[4] cerebral blood flow is higher than blood flow in the extra cerebral layers, thus increasing the available contrast in favour of DCS.

5. CONCLUSIONS

Characterization of the two independent modules demonstrate that the performances of TRS and DCS modules are in line with the state of the art for both these technologies. The results collected in this deliverable are the basis for the construction of a benchmark for the evaluation of the final prototype.

References:

[1] A. Pifferi et al. “Performance assessment of photon migration instruments: the MEDPHOT protocol” App.Opt. 44(1), p.p. 2104-2114

[2] H. Wabnitz et al. “Performance assessment of time-domain optical brain imagers, part 2: nEUROPt protocol” J Biomed Opt. 2014 19(8):086012

[3] Ijichi, S., Kusaka, T., Isobe, K., et al. (2005). Developmental changes of optical properties in neonates determined by near-infrared time-resolved spectroscopy. Pediatric research, 58(3), 568-573.

[4] Selb, J., Boas, D., Chan, et al. (2014, April). Sensitivity of Continuous-Wave NIRS and Diffuse Correlation Spectroscopy to Cerebral Hemodynamics during Hypercapnia. In Biomedical Optics (pp. BT5B-6). Optical Society of America.

[5] Buckley, E. M., Goff, D. A., Durduran, T., et al. (2010, April). Post-Surgical Cerebral Autoregulation in Neonates with Congenital Heart Defects Monitored With Diffuse Correlation Spectroscopy. In Biomedical Optics (p. BSuD71). Optical Society of America.

[6] Buckley, E. M., Hance, D., Pawlowski, T., et al. (2012). Validation of diffuse correlation spectroscopic measurement of cerebral blood flow using